Effect of Replacement of As by Ge and Sb on the Photo-Response under Near Infrared Femtosecond Laser Irradiation in As-based Sulfide Glasses

J. David Musgraves,* Nathan Carlie, Laeticia Petit, and Kathleen Richardson

School of Materials Science and Engineering/COMSET, Clemson University, Clemson, South Carolina 29634

Georges Boudebs

Laboratoire des Proprietes Optiques des Materiaux et Applications, FRE CNRS 2988, Universite d'Angers 2, Boulevard Lavoisier, 49045, Angers Cedex 01, France

Jiyeon Choi and Martin Richardson

College of Optics, Center for Research and Education in Optics and Lasers (CREOL), University of Central Florida, Orlando, Florida 32816

Bulk glasses having the compositions $As_{42}S_{58}$, $As_{36}Sb_6S_{58}$, and $As_{36}Ge_6S_{58}$ have been irradiated at 800 nm using a femtosecond-pulsed laser to determine the relationship between composition and photo-response. Localized variation in the glass volume (photo-expansion) has been determined through interferometric measurements of surface exposures, whereas induced refractive index change (photo-darkening) was determined from the diffraction efficiency of subsurface direct-written phase gratings. To understand the compositional dependence of the photo-response, the linear and nonlinear optical properties and structure of the unexposed glasses have been compared. The ablation threshold is shown to be controlled by variation of the nonlinear absorption, related to shifts of the absorption band gap with exchange of As by Ge or Sb. Changes in the unexposed network structure show that partial replacement of As by Ge or Sb induces an increased number of As–As bonding defects in the glass, particularly in the form of As_4S_4 molecular units which become polymerized into the network, impacting the photo-modification process. The Ge was found to induce an increase in the ablation threshold, and enhance both photo-darkening and photo-expansion effects, whereas Sb was shown to decrease ablation threshold and inhibit photo-darkening while enhancing photo-expansion.

Introduction

Chalcogenide glasses (ChGs) have been studied extensively for next-generation optical applications, such as Raman gain,[1] super-continuum generation,[2] and for use as microstructured fiber.[3] They possess excellent infrared transparency, large linear and nonlinear refractive indices, low phonon energies, and their properties are tunable through compositional tailoring. The high transparency of these glasses in the infrared[4] also leads to possible applications in optical molecular sensing, as most organic substances and functional groups have signature absorptions in this spectral region. Combined with ease of processing, these attributes make ChGs good candidates for near-, mid-, and long-wave infrared (IR) applications as compared with oxide glasses and single crystals, despite their often limited thermal and mechanical stability. For the purposes of device design, it may be necessary to tailor certain optical or thermal properties, as well as the photo-response of the glass when used for waveguide fabrication.

In contrast to the most standard fabrication techniques, direct laser writing (DLW) using ultrashort pulse lasers allows single-step production of waveguides, without the design and fabrication of a mask. A large number of photonic devices, including channel waveguides and Y couplers,[5] directional couplers,[6,7] tubular waveguides,[8] and active waveguides[9] have been successfully fabricated using this technique. Near-IR (NIR) ultrashort-pulsed lasers operate at photon energies far below the material bandgap energy, resulting in modification through multiphoton ionization.[5] As the material is essentially transparent to the writing wavelength, NIR femtosecond direct laser writing allows volumetric processing to depths limited only by the working distance of the focusing element. Hence, three-dimensional (3D) structures can be produced.[10] However, this technique requires that the refractive index of the materials locally increase upon exposure for such structures to guide light. Glasses in the As–S-based glasses have been shown by many authors[5,10–17] to be suitable for direct laser writing of optical elements as they exhibit an increase of the refractive index after light exposure. Partial replacement of As by Ge in this system has been shown to improve glass stability[18,19] and while less widely studied,[20,21] similar compositional tailoring is also possible in the As–Sb–S system.

In this article, we study the variation of photo-response for bulk glasses with compositions $As_{42}S_{58}$, $As_{36}Sb_6S_{58}$, and $As_{36}Ge_6S_{58}$ under NIR femtosecond irradiation. In addition to the improvements in glass stability for application purposes,[18–21] the impact of these compositional substitutions is interesting from a fundamental standpoint, where very little information exists on the literature on how Ge and Sb additions in arsenic sulfide base glasses affect the physical and optical properties. The current work focuses on the limited substitution of Ge and Sb into the base glass to understand these changes as perturbations from the base glass behavior; higher concentrations of Ge or Sb would be expected to dramatically change these behaviors. We report on characterization of the linear and nonlinear optical properties of the glasses and discuss their impact on the photo-sensitivity. Micro-Raman spectroscopy was employed to explore the structural modification induced to the glasses by laser irradiation. Hence, we examine the material response in the bulk glasses as a function of the glass composition to elucidate the structural mechanism behind the photo-response. Understanding the relationship between the optical properties, structure, and response of the glass under laser irradiation is a prerequisite toward the successful development of laser waveguide writing in these materials.

Experimental Procedure

Glass preparation

Bulk glasses with composition $As_{42}S_{58}$, $As_{36}Sb_6S_{58}$, and $As_{36}Ge_6S_{58}$, were prepared in 10-g batches. The glasses were melted from high purity elements (As: Alfa-Aesar 99.999% Ge: Sigma-Aldrich 99.999%, Sb: Alfa-Aesar 99.999%, and S: Cerac 99.999%). Prior to sealing and melting, the ampoule and batch were preheated to 100°C for 4 h while under high vacuum, to remove surface moisture from the quartz ampoule and the batch materials. The evacuated ampoule was then sealed with a gas-oxygen torch and heated to 850°C for 15 h. A rocking furnace was used to homogenize the melt, and melt-containing ampoule was then quenched in air to room temperature. Glass ingots were subsequently returned to the furnace for annealing for 15 h at 40°C below the glass transition temperature (T_g) of the glass. Bulk glasses were cut, polished, and optically examined for homogeneity. Elemental analysis was also performed using energy dispersive X-ray spectroscopy (EDS) to confirm that the correct glass composition was preserved throughout the process.

Characterization of the linear and nonlinear optical properties

The density of the bulk glasses was measured to be within ±0.02 g/cm^3 using Archimedes method with diethyl phthalate as the liquid medium. Absorption band gap values for the unexposed specimens were determined from ultraviolet to visible (Vis) absorption spectroscopy, taking the wavelength at which the absorption coefficient becomes greater than 10/cm.

Linear refractive index measurements over the range of 0.6–10.6 μm were carried out using a custom-modified commercial prism coupler instrument (Metricon model 2010, Metricon Corporation, Pennington, NJ). In addition to the standard 633-nm HeNe laser, four additional sources were added: a 1.547-μm telecom distributed feedback (DFB) fiber laser (Agilent Technologies, Santa Clara, CA), a 3.391-μm IR HeNe laser, a DFB quantum cascade laser operating at 5.348 μm (Maxion Technologies, College Park, MD), and a tunable CO_2 waveguide laser with a range of 9.3–10.6 μm. While the standard Ge photo-detector was suitable for the Vis–NIR wavelengths, the mid-IR wavelengths required the use of a room temperature Mercury–Cadmium–Zinc Telluride (MCZT) detector (Vigo systems, model PVM-10.6, Ożarów, Poland). The IR optical signal was chopped at 2 kHz and the signal was regenerated using a lock-in amplifier to decrease the signal-to-noise ratio. Gallium phosphide was used as the prism material due to its compatible refractive index and transparency window. This allowed the determination of refractive index within ±0.0004 refractive index units. Refractive index of the samples was calculated from intensity-angle plots using the method previously developed by Kirsch.[22]

Nonlinear refractive index measurements were performed using a modified Z-scan technique (using a 4-f imaging system), described earlier in detail.[23,24] Excitation was provided by a Nd:YAG laser delivering linearly polarized 15 ps single pulses at $\lambda = 1064$ nm with a 10-Hz repetition rate. Nonlinear acquisition was performed at a peak intensity of 1.3 GW/cm^2. The focal length used was 20 cm, and the beam waist at the focal plane was $\omega_0 = 30$ μm, giving a Rayleigh range $z_0 = \pi\omega_0^2/\lambda = 2.6$ mm. This value is larger than the sample thickness (typically 1 mm). Two sets of data acquisition (in the linear and the nonlinear regimes) allowed the opportunity to correct for inhomogeneities and surface imperfections in the sample. Measurements were repeated at least twice, illuminating the sample on the same position with different laser intensities to verify that no permanent photo-modification of the glasses occurred during the measurements.

Femtosecond laser irradiation

The laser system used for irradiation of the glass samples was a custom-built, extended cavity Ti:Sapphire oscillator with 26 MHz rep rate at 800 nm center wavelength. The oscillator produced maximum pulse energy of 21 nJ with a 5% pulse-to-pulse stability and a pulse width of 41 fs, which was measured using a Model 8-20 Grenouille (Swamp Optics, Atlanta, GA). A 10× (NA = 0.25) objective lens was used to focus a laser beam with the beam diameter of 4 μm onto samples mounted on the computer-controlled 3D translation stage (VP-25XA; Newport), and the irradiance was controlled using a neutral density filter. To obtain photo-induced structures of good quality, we first determined the irradiance threshold between material ablation and photo-induced structural modification[25] by independently increasing the laser intensities and exposure times, and examining the qualitative material response in terms of volume and refractive index changes.

Characterization of irradiated structures

Before forming irradiated structures, the necessary laser power needed to achieve photo-modification without inducing damage was determined by examining the intensity-dependent ablation threshold. A series of single spots were irradiated on the surface of the glass with varying exposure time and laser power. At the highest powers, surface damage was induced whereas, below a certain level only an expansion of the surface is observed. All photo-modified structures were then written at 90% of the composition-dependent threshold between ablation and photo-modification.

Two different femtosecond laser-written structures were made at the surface of the (volume expansion) sample and ~200 μm below the surface (index change) of the glasses to investigate the effect of the laser irradiation on the glass structure as well as on the relaxation of the photo-induced structure.

To quantitate the change in refractive index induced by laser irradiation (Δn), 1.5 x 1.5 mm array lines with 20 μm periodicity were written in the bulk by focusing the laser 200 μm below the surface of the glass, and translating the sample at varying speeds, lead-

ing to variation in total fluence (dose). These arrays form linear diffraction gratings. Refractive index change was measured by passing a probe laser at 800 nm, with low power (~10 mW CW) both through an unirradiated area, and through the grating. By comparing the ratio of the laser power in the first-order diffracted spot with the power transmitted by the sample with no grating present, the photo-induced Δn of the grating was calculated from the following equation:[26]

$$\eta = \left(\frac{\pi \Delta n d}{\lambda}\right)^2 + \left(\frac{\Delta k d}{4}\right)^2 \quad (1)$$

where Δn is the photo-induced refractive index change, Δk is the photo-induced change in the extinction coefficient, d is the height of the laser-induced features, λ is the probe wavelength (800 nm), and η is the diffraction efficiency taken as the ratio of diffracted laser power divided by the input power. As the probe wavelength is much longer than the absorption band gap, the effects of any photo-induced Δk is expected to be smaller than the uncertainty of the measurement (±0.1/cm). The height of the lines (d) was then measured using a differential interference contrast (DIC) optical microscope.

Photo-induced volume changes are also known to occur during exposure of similar glasses;[5,15,27,28] however, buried structures cannot truly expand or contract due to confinement by the surrounding unexposed glass, and exposure is expected to result only in the formation of complex stress fields and local density changes. These concerns may be largely obviated by exposing the surface of the glass, where volume change may occur through expansion or contraction in the unconstrained vertical direction. Lines with a length of 200 μm were written using various translation speed (i.e., various laser doses) on the surface of the glass to quantitate the amplitude of the surface photo-expansion as a function of the laser dose and of the glass composition. The surface photo-expansion was measured using a NewView 6300 (Zygo Corporation, Middlefield, CT) interferometer microscope and confirmed using a μTA 2990 microthermal analyzer (T.A. Instruments, New Castle, DE), which was equipped with a standard Si AFM probe.

Structural characterization

The micro-Raman spectra for glasses prior to and after irradiation were recorded using a Renishaw system 2000 Raman microscope. This system has a typical resolution of 2–3/cm at room temperature and uses a confocal arrangement in backscattering geometry. The system consists of a holographic notch filter for Rayleigh rejection, a microscope equipped with 10×, 50×, and 100× objectives and a thermoelectrically cooled CCD detector, coupled through a 1200 mm/line grating. A 785-nm NIR diode laser was used for excitation with an incident power of ~5 mW. The use of a 785-nm source with a low power and long integration times was specific to our study to avoid photo-structural changes in the samples which can be induced by the laser during measurement.

To examine the interdependence of the various changes to the Raman spectra before and after irradiation, the various bands have been deconvolved and their statistical correlation was evaluated using the following relation:

$$\rho_{X,Y} = \frac{E[(X - \mu_X)(Y - \mu_Y)]}{\sigma_X \sigma_Y} \quad (2)$$

where E is the expected value operator (essentially the mean value in the limit of large statistical samples), X and Y are the variables, μ_X and μ_Y are the expected values of the variables X and Y, and σ_X and σ_Y are the standard deviations of the variables X and Y. Correlation coefficients were calculated using Origin software. In the current case, we are considering the correlation between the relative areas of the fitted bands to each other and to the photo-expansion heights. A strong correlation (ρ close to +1 or −1) indicates that a change in the component of the glass strongly correlates to a change in the property of interest. A ρ-value of +1 would indicate that an increase in one feature correlates perfectly to an increase of another, whereas a ρ-value of −1 would indicate that an increase in the component should correlate perfectly to a decrease in the value of the property. A ρ-value of 0 indicates that no correlation exists between the component and the physical property. For five-sample data set with a 5% level of significance, a ρ-value of at least 0.88 is required to accept any X and Y as strongly correlated.[29]

Results

Replacement of As by Ge or Sb in bulk glass

Table I summarizes the density, band gap, and nonlinear optical properties of the bulk glasses with the

Table I. Summary of Glass Density, Band Gap, Calculated Electron Lone Pair Density, and Nonlinear Optical Properties

Nominal composition	$As_{42}S_{58}$	$As_{36}Ge_6S_{58}$	$As_{36}Sb_6S_{58}$
Density (±0.02) g/cm^3	3.20	3.15	3.41
Absorption edge (α = 10/cm) (±10) nm	580	570	630
Electron lone pair concentration x10^{-22}/cm^3	6.08	5.77	6.12
Nonlinear index: n_2 (1064 nm) x10^{-18} m^2/W	3.8 ± 0.6	3.2 ± 0.8	4.7 ± 0.8
$n_2/n_{2silica}$ (±10)	127	107	157
Nonlinear absorpton: β x10^{-12} m/W	2 ± 1	<1	4.5 ± 1.5
Figure of merit; $F = 2\beta\lambda_g/n_2$	1.1	0.7	2
Ablation threshold (GW/cm^2)	446 (±22)	485 (±25)	297 (±15)

compositions $As_{42}S_{58}$, $As_{36}Ge_6S_{58}$, and $As_{36}Sb_6S_{58}$. The linear refractive index dispersion curves of the bulk glasses, determined using prism coupling from 0.6 to 10.6 μm, are shown in Fig. 1. The replacement of As with Ge causes the refractive index to decrease while it increases when As is replaced by Sb. The replacement of As by Sb was found to induce a shift of the absorption band gap from ~580 to 630 nm, and to increase the glass' nonlinear refractive index (n_2) from 3.8 (±0.6) to 4.7 (±0.8) x 10^{-18} m^2/W and nonlinear absorption (β) from 2 (±1) to 4.5 (±1.5) x 10^{-12} m/W. In comparison, Ge was found to induce a slight blue shift of the band gap, and to decrease n_2 and β to 3.2 x 10^{-18} m^2/W and <1 x10^{-12} m/W, respectively.

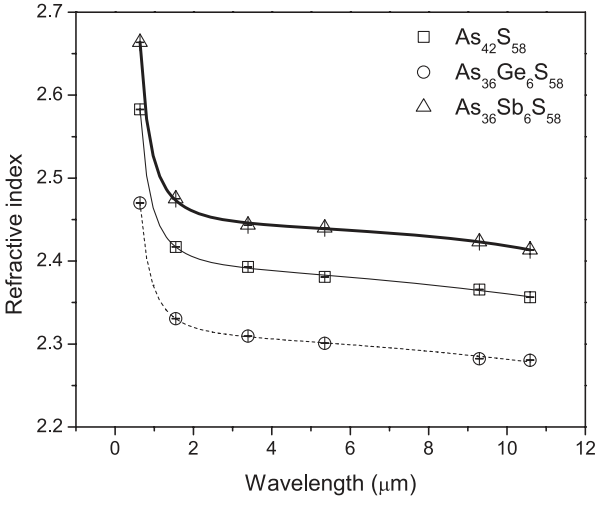

Fig. 1. Refractive index dispersion curves of bulk glasses as obtained using prism coupling, fit with Sellmeier dispersion curves.

The micro-Raman spectra of the nonirradiated bulks can be seen in Figs. 2–4, and the mode assignments in Table II. The main band of all three glasses is composed of three overlapping bands related to $AsS_{3/2}$ pyramidal units, including the symmetric and asymmetric stretches of the AsS_3 units at 310/cm and 345/cm, respectively,[30] and stretching motion of $S_{2/2}As–S–As–S_{2/2}$ centered around the bridging S at 380/cm. [30] Several additional small bands appear in the low wavenumber region (200–250/cm), which are related to As–As bonds either in $S_{2/2}As–As–S_{2/2}$ network units (220/cm)[10] or isolated As_4S_4 molecules (235/cm).[31,32] Finally, a small band near 490/cm can be seen in the spectrum of $As_{42}S_{58}$ (Fig. 2), which is related to S–S homopolar bonds in $S_{2/2}As–S–S–AsS_{2/2}$ disulfide bridges.[20] Upon replacement of As by Sb (Fig. 3), the main band broadens significantly and shifts to lower wavenumber, due to the introduction of a new band near 290/cm related to the symmetric stretch of SbS_3 pyramids.[30] Replacement of As by Ge (Fig. 4) sharpens the main band and shifts it slightly to higher wavenumbers, due to addition of a band corresponding to the symmetric stretch of $GeS_{4/2}$ tetrahedra at 340/cm;[33] a shoulder near 420/cm related to the stretch of $S_{3/2}Ge–S–GeS_{3/2}$ bridges[34] is also seen. The appearance of a shoulder of the main bands of both substituted glasses at 365/cm, corresponds to an increase of the band at 220/cm both attributed to As_4S_4.[31] A small band near 270/cm found only in the spectrum of $As_{36}Ge_6S_{58}$ is attributed to As_4S_3 units, also containing As–As bonds.[32]

Ablation threshold

To understand the mechanism underlying photoresponse, we must first know the maximum laser inten-

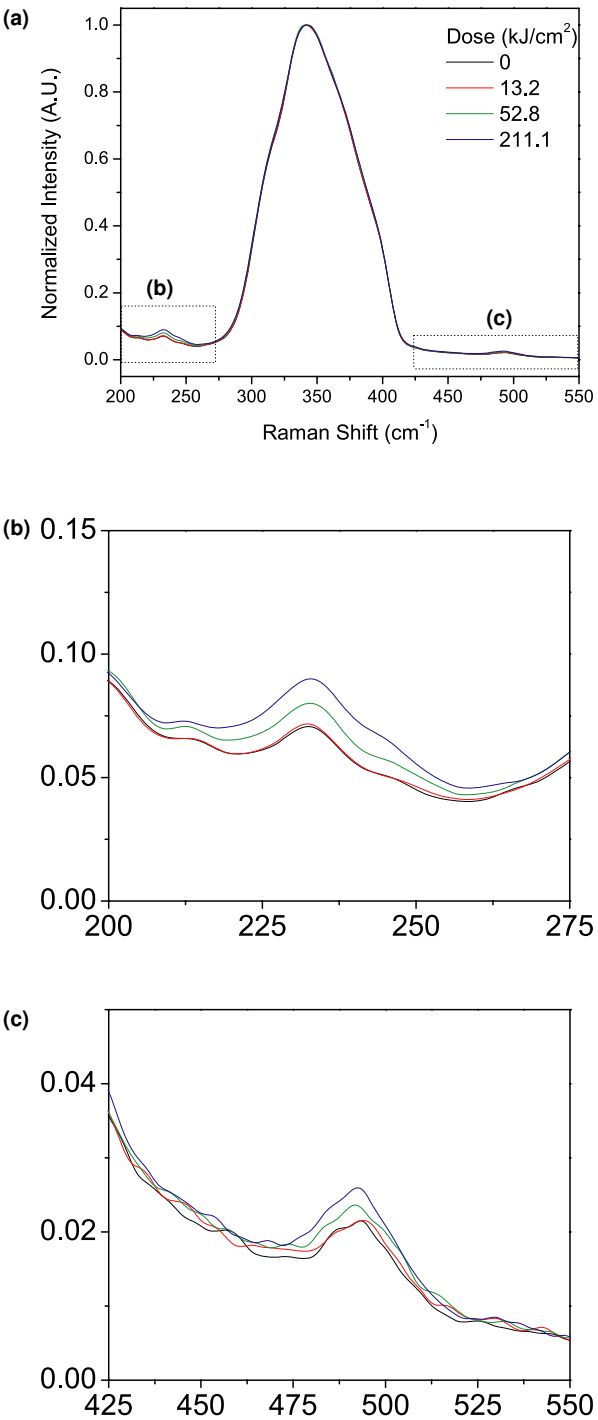

Fig. 2. Micro-Raman spectra of the $As_{42}S_{58}$ glass before and after irradiation at varying laser dose (a), with enlargements of the regions from 200/cm to 250/cm (b), and from 425/cm to 550/cm (c).

sity that the glass can handle without damage, as the peak intensity obtained from such short laser pulses can be high enough to cause ablation of the sample surface. The threshold between ablation and photo-modification was determined by independently increasing the laser intensity and exposure time until ablation was observed. In the present study, the largest laser irradiance which was found not to cause damage to the sample surface after a maximum exposure time of 100 ms was taken as the ablation threshold (I_a). The replacement of As by Sb was found to induce a large decrease in the I_a from 446 (±22) to 298 (±15) GW/cm^2, whereas the replacement of As by Ge caused a slight increase of I_a to 485 (±24) GW/cm^2; these values are included in Table I. As writing was performed at 90% of these values, the writing conditions used in this study were necessarily composition-dependent.

Photo-expansion and refractive index change

Lines were written at the surface and within the bulk of the glasses using various laser doses (translation speeds) at 90% of the ablation threshold. Using a New-View 6300 interferometric microscope, an expansion of the glass surface upon irradiation just below the ablation threshold was observed for all of the investigated compositions. Figure 5a summarizes the height of the photo-expanded areas as a function of incident dose. It is clearly shown that the photo-expansion of the glass depends on integrated dose, and that it is influenced by changes in composition. Figure 5a shows that the expansion initially increases linearly with increasing dose, but as the dose increases above ~100 kJ/cm^2, the rate of increase begins to slow. On replacement of As by Ge, the height of the photo-expansion increases from 30 nm to 52 nm at a dose of ~250 kJ/cm^2 whereas replacement by Sb only causes an increase up to 40 nm at a similar dose.

Figure 5b presents the variation of refractive index (Δn; as measured from the 800 nm diffraction efficiency of subsurface gratings) as a function of the laser dose. The laser irradiation was found to locally increase the refractive index linearly as a function of the laser dose. When irradiated at 90% of its ablation threshold with a dose of ~10 kJ/cm^2, the Δn in $As_{42}S_{58}$ was found to be 3.3 (±0.1) x 10^{-3}. For a similar dose, the Ge-containing glass exhibits the largest induced Δn and the Sb-containing glass inhibits the smallest induced Δn.

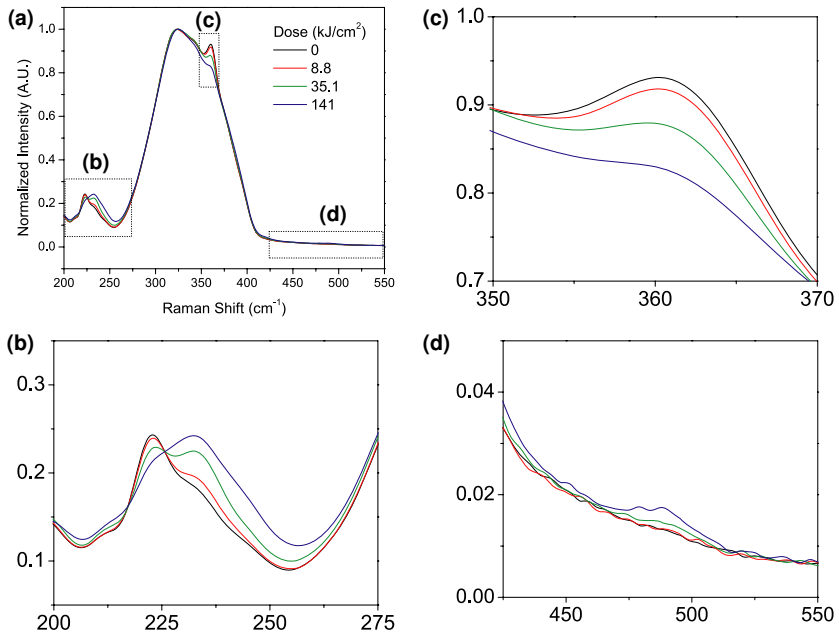

Fig. 3. Micro-Raman spectra of the $As_{36}Sb_6S_{58}$ glass before and after irradiation at varying laser doses (a), with enlargements of the regions from 200/cm to 250/cm (b), from 350/cm to 370/cm (c), and from 425/cm to 550/cm (d).

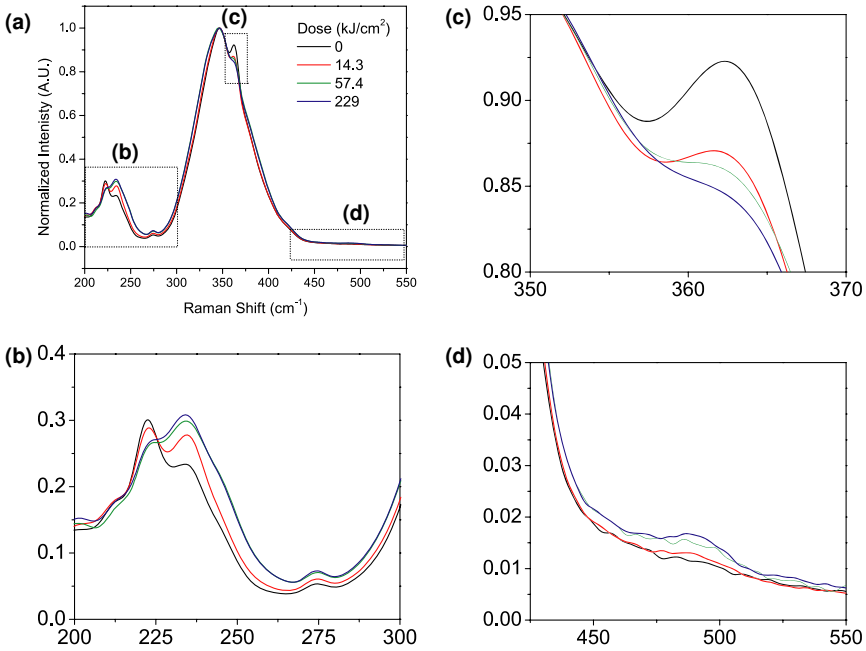

Fig. 4. Micro-Raman spectra of the $As_{36}Ge_6S_{58}$ glass before and after irradiation at varying laser doses (a), with enlargements of the regions from 200/cm to 250/cm (b), from 350/cm to 370/cm (c), and from 425/cm to 550/cm (d).

Table II. Raman Band Assignments for $As_{42}S_{58}$, $As_{36}Sb_6S_{58}$, and $As_{42}Ge_6S_{58}$ Bulk Glasses

Raman shift (per cm)	Assignment	References
210	B_1 stretching mode of As_4S_4 molecule	31
225	As–S–As bending (E) mode of As_4S_4	31
235	Stretching of $S_{2/2}As–AsS_{2/2}$ homopolar network bonds	10
270	A_1 mode of As_4S_3 molecule	31
310	Asymmetric stretching of $AsS_{3/2}$ network units	30
345	Symmetric stretching of $AsS_{3/2}$	30
365	A_1 breathing motion of As_4S_4 molecule	31
380	T_2 stretching motion of $S_2As–S–AsS_2$ network bridges	30
340	A_1 symmetric stretching mode of $GeS_{4/2}$ network units	32
420	T_2 stretching motion of $S_3Ge–S–GeS_3$ bridges	33
290	Asymmetric stretch of $SbS_{3/2}$ units	30
490	A_1 mode of S_n chains	20,47

Structural photo-modification

Due to the practical difficulty of focusing inside a buried structure to measure its Raman spectra without signal coming from the matrix, the Raman spectra of the irradiated glasses have been recorded only for surface exposures. Figures 2–4 display the micro-Raman spectra of the $As_{42}S_{58}$, $As_{36}Sb_6S_{58}$, and $As_{36}Ge_6S_{58}$ glasses, respectively, before and after irradiation using varying doses. When the laser dose increases for irradiation of the base glass ($As_{42}S_{58}$), a small but reproducible increase of intensity for the bands at 235/cm and 490/cm relative to the main band is seen. In comparison, the spectra of the $As_{36}Sb_6S_{58}$ and $As_{36}Ge_6S_{58}$ exhibit larger increases near 235/cm and the amplitude of the bands located near 225/cm and 365/cm (not present in the base glass) decreases. Moreover, in the spectra of the $As_{36}Ge_6S_{58}$ glass, the main band becomes broader with an increase of intensity for the shoulder near 420/cm after laser irradiation. A small increase in the amplitude of the S–S band at 490/cm is also seen for the two substituted glasses, although the magnitude of this change is close to noise in the spectra, and is similar to that of the base glass within ±10%.

Discussion

Ablation threshold

Irradiation in this study was performed well below the band gap, where the density of states resulting from the Urbach absorption tail[35] is expected to be small. Thus, the compositional dependence of the ablation threshold of the glass (I_a) may be expected to depend on variations of the nonlinear absorptivity (β). The value of β decreases and I_a increases slightly with Ge substitution, whereas Sb substitution induces a strong increase of β and similarly, large decrease of I_a. These variations in the nonlinear optical properties can be attributed to changes of proximity of the absorption band gap to the wavelength of the *Z*-scan measurement, and to the slight decrease of the electron lone pair concentration with Ge substitution,[36] as shown in Table I.

Structural analysis of the unexposed glasses

The observation that a decrease of the glass density (photo-expansion) corresponds with an increase of the refractive index is superficially contradictory, as the Lorenz–Lorentz relation predicts that density and refractive index are directly related.[37] This suggests that, in addition to the volume expansion, there is an electronic contribution to refractive index change through the Kramers–Kronig relation.[38] Recent publications[15,17,39] show that these two effects (volume change and index change) occur with different kinetics in the As–S and As–Se systems, leading to the conclusion that they, in fact, result from different mechanisms occurring separately during exposure. Indeed, as seen in Figs. 5a and b, substitution of As by Ge enhances both the expansion and darkening response, whereas Sb substitution enhances photo-expansion but inhibits photo-darkening.

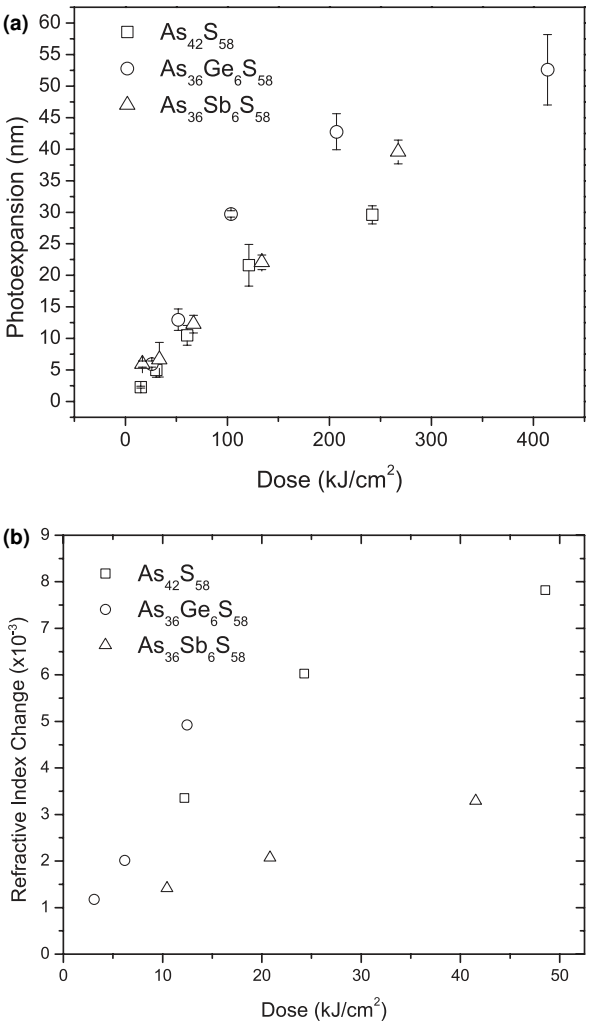

Fig. 5. Photo-expansion (a), photo-induced index change (b), and as a function of integrated laser dose, for $As_{42}S_{58}$, $As_{36}Ge_6S_{58}$, and $As_{36}Sb_6S_{58}$ glasses.

Thus, we may expect that the relative magnitudes of these two responses are composition-dependent.

To understand this compositional dependence, and the structural origin of the photo-response, it is first necessary to discuss the impact of glass chemistry on the unexposed structure. As noted before, the network of the base glass ($As_{42}S_{58}$) is composed primarily of interconnected $AsS_{3/2}$ units which are expected to form a two-dimensional sheet type structure;[40] however, a small number of homopolar "wrong" As–As was observed due to a slight stoichiometric excess of As in relation to S. As there are many ways to consider the bonding forms occurring within the glass, we believe that in the context of the current study, the most instructive may be to consider the molecular units. In the case of the base glass, the two fundamental molecular units are $AsS_{3/2}$ units, of which the network is comprised, and $AsS_{2/2}$ units, which are the basis for the "wrong" bonds in the glass. It can be seen that $S_{2/2}$ As–$AsS_{2/2}$ network homopolar bonds are formed of two $AsS_{2/2}$ units, and As_4S_4 molecules are formed of four of these units bonded together. As the S atoms are shared with neighboring units, each $AsS_{3/2}$ unit contains 1.5 effective S atoms whereas $AsS_{2/2}$ contains 1 S atom. The relative numbers of these units may then be unambiguously calculated from the composition by solving a set of linear equations. If X is defined as the number of $AsS_{3/2}$ units, and Y is defined as the number of $As_{2/2}$ units, then

$$X + Y = 42 \quad \text{(As atoms per 100)} \tag{3}$$

$$1.5X + Y = 58 \quad \text{(S atoms per 100)} \tag{4}$$

Solving these equations gives 32 $AsS_{3/2}$ units and 10 $AsS_{2/2}$ per 100 atoms, or 76% and 24%, respectively.

The As–As homopolar bonds have been shown to form preferentially over Ge–Ge or Sb–Sb homopolar bonds in ternary glasses,[18,19,30] primarily due to differences in bond energies[41] and in this case, also due to the relatively low concentration of Ge and Sb. We can therefore extend this calculation to the substituted glasses by assuming that only $SbS_{3/2}$ or $GeS_{4/2}$ units are added upon substitution, and letting the number of these units be given as the variable Z in

$$Z = 6 \tag{5}$$

$$X + Y = 36 \tag{6}$$

$$1.5X + Y + 1.5Z(SbS_{3/2}) = 58 \tag{7}$$

or

$$1.5X + Y + 2Z(GeS_{4/2}) = 58 \tag{8}$$

Solving for $As_{36}Sb_66_{58}$ (Eqs. (5–7)) gives 62% $AsS_{3/2}$, 24% $AsS_{2/2}$, and 14% $SbS_{3/2}$, whereas for $As_{36}Ge_6S_{58}$ (Eqs. (5), (6), and (8)), it gives 48% $AsS_{3/2}$, 38% $AsS_{2/2}$, and 14% $GeS_{4/2}$. From this, we can see that substitution decreases the number of fully coordinated As units which can be formed, thereby increasing the rela-

tive number of As–As homopolar bonds. Each $AsS_{3/2}$ unit contributes 3 As–S bonds to the network while each $AsS_{2/2}$ contributes 2 As–S and 0.5 As-As bonds, and hence the expected bond statistics may also be determined using this method, giving 4% As–As bonds in $As_{42}S_{58}$, 5% in $As_{36}Sb_6S_{58}$, and 8% in $As_{36}Ge_6S_{58}$. Finally, a third type of As-containing unit, S–$AsS_{2/2}$, should also be considered. Two of these units would be expected to form an S–S homopolar bond (in $S_{2/2}$ As–S–S–$As_{2/2}$), which may be expected in small concentrations due to randomization of bonding in the amorphous network. Each S–$AsS_{2/2}$ unit formed results in the formation of an additional $AsS_{2/2}$ unit. This is in good agreement with the evolution of the Raman spectrum of the glass with composition. It is also important to note that these additional As–As bonds found in the substituted glasses occur primarily as As_4S_4 molecules, as evidenced by the large intensity at 220/cm and 365/cm,[31] (and some As_4S_3 in the case of $As_{36}Ge_6S_{58}$), which are not present in significant quantities in the base glass.

Photo-induced structural effects

The spectra of the glasses before and after exposure have been deconvolved using Gaussian profiles, and Fig. 6 compares the relative areas (as compared with the unexposed values) from fitting two bands at 235/cm and 490/cm in $As_{42}S_{58}$ (from Figs. 2b and c) with the height of the photo-expansion. Peak areas have been preferred over intensities to account for changes in band widths. The integrated areas of the peaks are directly related to the number density of the scattering species present in the glass, thus by comparing changes in peak area, we can understand how the photo-modification process affects the various glass constituents. One can see from the figure that the relative area of both peaks increases with increasing expansion height (increasing dose), indicating that a larger number of As–As and S–S bonds are created as expected from previous work,[5] but the relation between peak areas and expansion height is not linear. Statistical analysis has demonstrated a ρ-value of 0.99 between the areas of the two bands, but below 0.9 between the band areas and the expansion height. This suggests that the changes in peak areas are strongly correlated to each other, and are likely mechanistically linked; however, homopolar bond concentration and expansion height are only weakly correlated, and a second structural modification may cause, or at least contribute to, the expansion of glass surface.

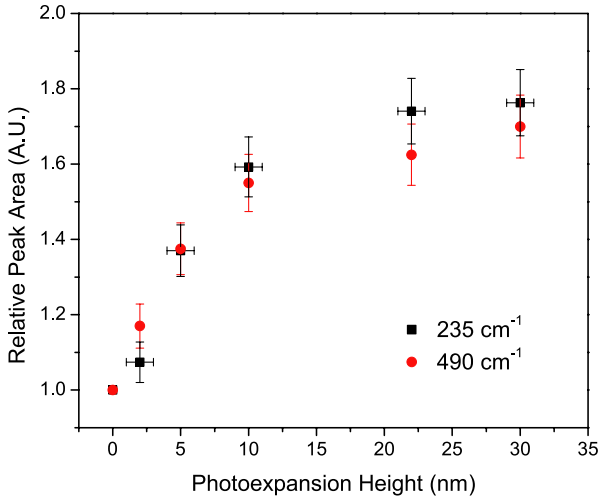

Fig. 6. Relative peak areas for 235/cm and 490/cm of $As_{42}S_{58}$ as a function of photo-expansion height for surface irradiations with varying translation speeds.

It is important to note, that surface expansion values should be normalized to the exposed volume to have a true estimate of the relative photo-induced volume change; however, the irradiation conditions were identical for each exposed line (only translation speed was changed), meaning that the exposed volume should also be constant. As the correlation coefficient is not influenced by normalization of the input values, our conclusion would not be changed. Some small variation in the shape of the main band was also observed (Fig. 2a), and is probably related to a change in bond angles or torsions within the As–S network, resulting in volume change,[28] but this could not be deconvolved in our case. Some authors have suggested that photo-oxidation plays a role; however, this has only been shown in low-intensity band gap irradiation with long exposure times[41,42] and there may not be sufficient time for significant oxygen diffusion during these short (0.02–1 s) NIR exposures. This leads us to suggest that in the base glass, modification proceeds through photolytic cleavage of As–S bonds in $AsS_{3/2}$ units, leading to the formation of $AsS_{2/2}$ and S–$AsS_{2/2}$ units (As–As and S–S bonds), as shown by previous authors,[5,10,43] but that an additional deformation of network may contribute to photo-expansion.

In comparison with the base glass, the spectra of the substituted glasses (Figs. 3 and 4) display significantly higher areas for the peaks near 220/cm

and 365/cm, attributed to As_4S_4, in the unexposed state. During irradiation, the area of these two peaks (b and c) decreases dramatically, and the area of the band near 235/cm (b) increases, along with a much smaller increase of the band at 490/cm (d). It should be noted that the increase of the S–S band (490/cm) following irradiation is of a similar magnitude for these two glasses as that observed for the base glass. Thus, we can expect that a small portion of the increased intensity at 235/cm can be attributed to photolytic cleavage of the As–S network to yield $S_{2/2}As–S–S–AsS_{2/2}$ and $S_{2/2}As–AsS_{2/2}$, as observed for the base glass; however, this effect is too small to lead to the large variations at 235/cm in the spectra of the substituted glasses.

The relative areas of the bands at 220, 235, and 365/cm for $As_{36}Sb_6S_{58}$ (Figs. 3b and c) and $As_{36}Ge_6S_{58}$ (Figs. 4b and c) are compared as a function of the expansion height in Figs. 7a and b, respectively. One can see from the figure that as the relative area of the band at 235/cm increases, those of the two peaks related to As_4S_4 decrease simultaneously for both of the substituted glasses. Statistical analysis has shown that the ρ-value relating the area of the two As_4S_4 bands to each other is greater than 0.99 and those relating the areas of these bands to the $S_{2/2}As–AsS_{2/2}$ homopolar network bond at 235/cm are below −0.98. This indicates that there is a very strong correlation between both bands attributed to As_4S_4 and a strong negative correlation between As_4S_4 and As–As network units, suggesting that both As–As network bond creation and As_4S_4 destruction are linked. Moreover, the total area between 210/cm and 250/cm is approximately constant, indicating that the total number of As–As bonds relative to As–S does not change significantly (excluding a similar small increase linked to S–S bond formation as seen for $As_{42}S_{58}$). One possible interpretation of this behavior is the mechanism proposed in Fig. 8.

From the figure, network As–S bonds are broken during photo-irradiation, resulting in formation of an electron-hole pair, in agreement with previous electron-spin studies.[44] These may remain after exposure and recombine to form the original bond, or lead to bond rearrangement resulting in polymerization of the As_4S_4 molecule into the network. It is also possible for a similar mechanism to proceed through a radical intermediate; however, it is not the reaction path, but the end product which we consider herein. To verify that such a structural change would result in the observed variations in the Raman spectra, the spectra of the As_4S_4

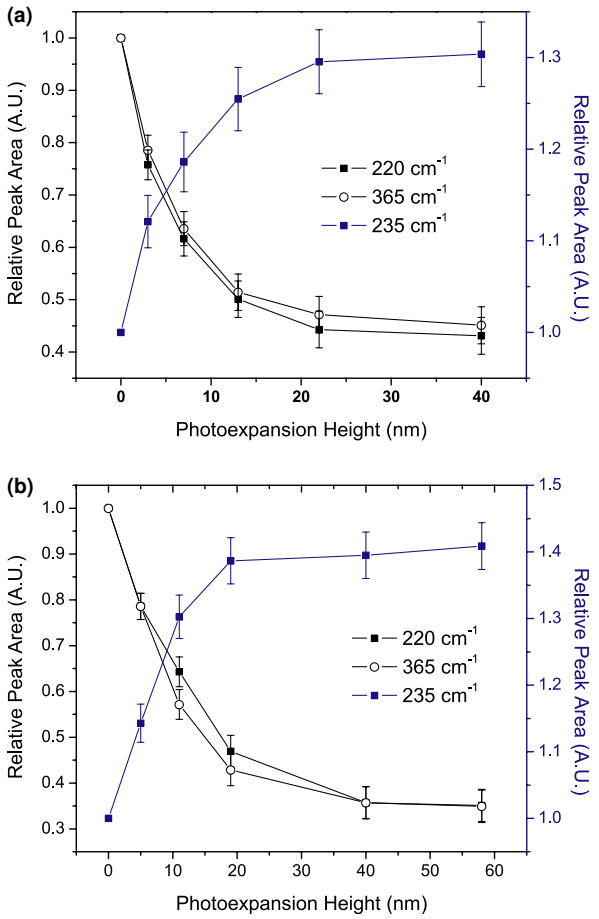

Fig. 7. Relative peak areas for 220/cm, 235/cm, and 490/cm of $As_{36}Sb_6S_{58}$ (a) and $As_{36}Ge_6S_{58}$ (b) as a function of photo-expansion height for surface irradiations with varying translation speeds.

molecule and the proposed reaction product shown in the figure were calculated using a density functional theory model. Spectra were generated from geometry-optimized structures through a normal mode analysis routine using the Gaussian 03 package, and employing the B3LYP hybrid functional and a 6-311* basis set. The calculated spectra for As_4S_4 and the predicted polymerized structure (showing the calculated frequencies of the modes with arbitrary intensities) are shown in Fig. 9. One can see from the figure that the sharp feature near 365/cm shifts to 355/cm and becomes broader as it is associated with motions of the connected network, whereas the feature near 220/cm splits into two modes near 220/cm and 250/cm. These

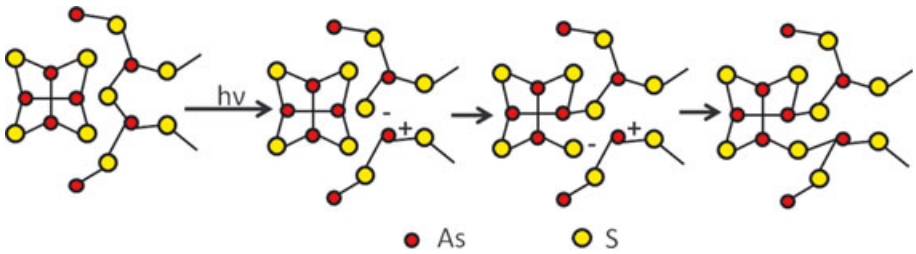

Fig. 8. Proposed mechanism for polymerization of As_4S_4 cluster into the glass network during irradiation.

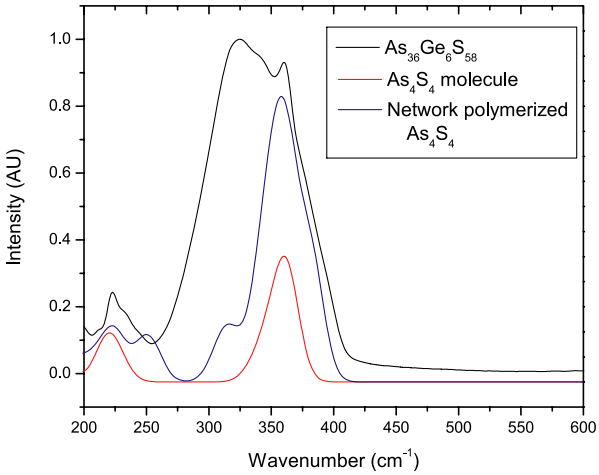

Fig. 9. Simulated Raman spectra of As_4S_4 molecule and polymerized network product, modeled using density functional theory.

results favorably reproduce the observed changes in the Raman spectra of the substituted glasses, and support our conclusions concerning the structural changes. As a result of this polymerization response, the presence of large numbers of As_4S_4 in the substituted glasses significantly changes the photo-modification mechanism.

It is important to reiterate that the observed photo-expansion and refractive index changes are not explained by such a mechanism alone. For instance, the index change observed in $As_{36}Sb_6S_{58}$ is much smaller in relation to the photo-expansion, when compared with $As_{36}Ge_6S_{58}$. It is also important to note that, as with the base glass, the correlation coefficients between the bands related to As–As bonds and the expansion height are all below 0.9, indicating that there is likely an additional mechanism involved the expansion of the glass, which has been proposed by some authors as a distortion of bonding within the network or variation of interplane spacing between two-dimensional $AsS_{3/2}$ sheets.[45] This network bond modification is clearly visible in the spectrum of $As_{36}Ge_6S_{58}$ as a broadening of the main band and shift to lower wavenumber, which is caused likely by modification of the bonding around GeS_4 tetrahedra.[46,47] Unfortunately, due to the large number of overlapping features in Raman spectra of these glasses, deconvolution of variations in the main bands was not possible. Additional insight may be provided by neutron or X-ray scattering studies, such as extended X-ray absorption fine structure, provided they allow sufficient spatial resolution, however, such techniques are not available to the authors of this work.

Conclusion

We have demonstrated that substitution of As for Sb or Ge in $As_{42}S_{58}$ bulk glasses results in modification of the linear and nonlinear optical properties and structure, leading to different photo-responses under 800 nm femtosecond irradiation. Addition of Sb induces a red shift of the band gap, and an increase of the linear (n) and nonlinear (n_2) refractive index and two-photon absorptivity (β), whereas Ge induces a slight blue shift of the band gap and decreases in n, n_2, and β. The Ge was also found to enhance photo-expansion and photo-darkening, whereas Sb increases expansion, but decreases the magnitude of the index change. Substitution of either element causes an increase in the number of As–As bonding defects in the unexposed glass, primarily in the form of As_4S_4 molecules. As irradiation of the $As_{42}S_{58}$ base glass causes photolytic cleavage of the As–S network to form As–As and S–S bonds, irradiation of the substituted glasses causes an additional polymerization of As_4S_4 into the

glass network. These structural modifications alone were found to be inadequate to explain the observed composition variations in the photo-expansion, and photo-darkening, which are believed to be effected by additional modifications of the glass network.

References

1. R. Stegeman, *et al.*, "Raman Gain Measurements and Photo-Induced Transmission Effects of Germanium- and Arsenic-based Chalcogenide Glasses," *Opt. Express*, 14 [24] 11702–11708 (2006).
2. A. B. Seddon, "Chalcogenide Glasses – A Review of their Preparation, Properties and Applications," *J. Non-Cryst. Solids*, 184 44–50 (1995).
3. O. Fedotova, A. Husakou, and J. Herrmann, "Supercontinuum Generation in Planar Rib Waveguides Enabled by Anomalous Dispersion," *Opt. Express*, 14 [4] 1512–1516 (2006).
4. G. Delaizir, P. Lucas, X. Zhang, H. Ma, B. Bureau, and J. Lucas, "Infrared Glass-Ceramics with Fine Porous Surfaces for Optical Sensor Applications," *J. Am. Ceram. Soc.*, 90 [7] 2073–2077 (2007).
5. A. Zoubir, *et al.*, "Direct Femtosecond Laser Writing of Waveguides in As2S3 Thin Films," *Opt. Lett.*, 29 [7] 748–750 (2004).
6. D. Homoelle, S. Wielandy, A. L. Gaeta, N. F. Borrelli, and C. Smith, "Infrared Photosensitivity in Silica Glasses Exposed to Femtosecond Laser Pulses," *Opt. Lett.*, 24 [18] 1311–1313 (1999).
7. A. M. Streltsov and N. F. Borrelli, "Fabrication and Analysis of a Directional Coupler Written in Glass by Nanojoule Femtosecond Laser Pulses," *Opt. Lett.*, 26 [1] 42–43 (2001).
8. A. Zoubir, C. Lopez, M. Richardson, and K. Richardson, "Femtosecond Laser Fabrication of Tubular Waveguides in Poly(methyl methacrylate)," *Opt. Lett.*, 29 [16] 1840–1842 (2004).
9. R. Osellame, *et al.*, "Femtosecond Writing of Active Optical Waveguides with Astigmatically Shaped Beams," *J. Opt. Soc. Am. B*, 20 [7] 1559–1567 (2003).
10. M. Frumar, Z. Polak, and Z. Cernosek, "Raman Spectra and Photostructural Changes in the Short-Range Order of Amorphous As-S Chalcogenides," *J. Non-Cryst. Solids*, 256&257 105–110 (1999).
11. M. Bertolotti, F. Michelotti, V. Chumash, P. Cherbari, M. Popescu, and S. Zamfira, "The Kinetics of Laser-Induced Structural-Changes in As_2S_3 Amorphous Films," *J. Non-Cryst. Solids*, 192&193 657–660 (1995).
12. S. Juodkazis, T. Kondo, H. Misawa, A. Rode, M. Samoc, and B. Luther-Davies, "Photo-Structuring of As2S3 Glass by Femtosecond Irradiation," *Opt. Express*, 14 [17] 7751–7756 (2006).
13. V. K. Tikhomirov, *et al.*, "Non-Linear Raman Effects and Photodarkening in Chalcogenide Glass As_2S_3," *Europhys. Lett.*, 76 [2] 312–317 (2006).
14. V. Lyubin, M. Klebanov, L. Shapiro, M. Lisiansky, B. Spektor, and J. Shamir, "Peculiarities of Photorefraction Effect in Thick Glassy As2S3 Films," *J. Optoelectron. Adv. Mat.*, 1 [3] 31–35 (1999).
15. K. Tanaka, "Photoexpansion in As_2S_3 Glass," *Phys. Rev. B*, 57 [9] 5163–5167 (1998).
16. A. Ganjoo, *et al.*, "Planar Chalcogenide Glass Waveguides for IR Evanescent Wave Sensors," *J. Non-Cryst. Solids*, 352 [6–7] 584–588 (2006).
17. A. Ganjoo and H. Jain, "Millisecond Kinetics of Photoinduced Changes in the Optical Parameters of a-As2S3 Films," *Phys. Rev. B*, 74 [2] 024201 (2006).
18. K. Tanaka, "Structural Phase Transitions in Chalcogenide Glasses," *Phys. Rev. B*, 39 [2] 1270–1279 (1989).
19. B. G. Aitken and C. W. Ponader, "Physical Properties and Raman Spectroscopy of GeAs Sulphide Glasses," *J. Non-Cryst. Solids*, 256&257 143–148 (1999).
20. M. Kincl and L. Tichy, "Some Physical Properties of $Ge_xAs_xS_{1-2x}$ Glasses," *Mater. Chem. Phys.*, 103 [1] 78–88 (2007).
21. Q. Liu, X. Zhao, K. Tanaka, A. Narazaki, K. Hirao, and F. Gan, "Second Harmonic Generation in Ge-As-S Glasses by Electron Beam Irradiation and Analysis of the Poling Mechanism" *Opt. Comm.*, 198 [1–3] 187–192 (2001).
22. S. T. Kirsch, "Determining the Refractive Index and Thickness of Thin Films from Prism Coupler Measurements," *Appl. Opt.*, 20 [12] 2085–2089 (1981).
23. M. Sheik-Bahae, A. A. Said, T. H. Wei, D. Hagan, and E. W. V. Stryland, "Three-Photon Absorption in InAs," *IEEE J. Quantum Electron.*, 26 [4] 760–769 (1990).
24. G. Boudebs and S. Cherukulappurath, "Nonlinear Refraction Measurements in Presence of Nonlinear Absorption Using Phase Object in a 4f System," *Opt. Comm.*, 250 [4–6] 416–420 (2005).
25. T. Anderson, *et al.*, "Femtosecond Laser Photo-Response of $Ge_{23}Sb_7S_{70}$ Films," *Opt. Express*, 16 [24] 20081–20098 (2009).
26. H. J. Eichler, P. Gunter, and D. W. Pohl, *Laser Induced Dynamic Gratings*, Springer-Verlag, Berlin, 1986.
27. M. Frumar, Z. Cernosek, J. Jedelsky, B. Frumarova, and T. Wagner, "Photoinduced Changes of Structure and Properties of Amorphous Binary and Ternary Chalcogenides," *J. Optoelectron. Adv. Mater.*, 3 [2] 177–188 (2001).
28. W. Zhou, M. A. Paesler, and D. E. Sayers, "Structure and Photoinduced Structural-Changes in a-As_2S_3 Films – A Study by X-ray Absorption Fine Structure," *Phys. Rev. B*, 46 [7] 3817–3825 (1992).
29. R. Caulcutt and R. Boddy, *Statistics for Analtical Chemists*, Chapman and Hall, New York, 1983.
30. E. I. Kamitsos, J. A. Kapoutsis, I. P. Culeac, and M. S. Iovu, "Structure and Bonding in As-Sb-S Chalcogenide Glasses by Infrared Reflectance Spectroscopy," *J. Phys. Chem. B*, 101 [51] 11061–11067 (1997).
31. A. Bertoluzza, C. Fagnano, P. Monti, and G. Semerano, "Raman and Infrared Spectra of As_2S_x Chalcogenide Glasses with $x \leq 3$," *J. Non-Cryst. Solids*, 29 [1] 49–60 (1978).
32. C. Julien, *et al.*, "Raman and Infrared Spectrscopic Studies of Ge-Ga-Ag Sulfide Glasses," *Mater. Sci. Eng. B* 22 [2–3] 191–200 (1994).
33. Q. Mei, J. Saienga, J. Schrooten, B. Meyer, and S. W. Martin, "Preparation and Characterization of Glasses in the $Ag_2S+B_2S_3+GeS_2$ System," *J. Non-Cryst. Solids*, 324 [3] 264–276 (2003).
34. S. R. Elliot, *Physics of Amorphous Materials*, Longman, Essex, 1990.
35. L. Petit, *et al.*, "Correlation between the Nonlinear Refractive Index and Structure of Germanium-based Chalcogenide Glasses," *Mater. Res. Bull.*, 42 [12] 2107–2116 (2007).
36. D. E. Aspnes, "Local Field Effects and Effect Medium Theory – A Microscopic Perspective," *Am. J. Phys.*, 50 [8] 704–709 (1982).
37. J. S. Toll, "Causality and the Dispersion Relation: Logical Foundations" *Phys. Rev.*,104 1760–1770 (1956).
38. K. Antoine, H. Jain, and M. Vlcek, "Optical Spectroscopy of a-As_2Se_3 under *in situ* Laser Irradiation," *J. Non-Cryst. Solids*, 2006 [352] 595–600 (2006).
39. P. Bonazzi and L. Bindi, "A crystallographic Review of Arsenic Sulfides: Effects of Chemical Variations and Changes Induced by Exposure to Light," *Z. Kristallogr.*, 223 [1–2] 132–147 (2008).
40. Y. Luo, *Comprehensive Handbook of Chemical Bond Energies*, CRC Press, Boca Raton, FL, 2007.
41. M. Popescu, "Chalcogenides – Past, Present, Future," *J. Non-Cryst. Solids*, 352 [26–27] 887–891 (2006).
42. E. Marquez, A. M. Bernal-Oliva, J. M. Gonzalez-Leal, R. Prieto-Alcon, and T. Wagner, "Optical Properties and Structure of Amorphous $(As_{0.33}S_{0.67})_{(100-x)}Te_x$ and $Ge_xSb_{40-x}S_{60}$ Chalcogenide Semiconducting Alloy Films Deposited by Vacuum Thermal Evaporation," *J. Phys. D.*, 39 [9] 1793–1799 (2006).
43. O. Efimov, *et al.*, "Waveguide Writing in Chalcogenide Glasses by a Train of Femtosecond Laser Pulses," *Opt. Mater.*, 17 [3] 379–386 (2001).
44. J. Hautala, W. D. Ohlsen, and P. C. Taylor, "Optically Induced Electron Spin Resonance in As_xS_{1-x}," *Phys. Rev. B*, 38 [16] 11048–11060 (1988).
45. M. Popescu and W. Hoyer, "Structural Features and Mechanism of Reversible Photoinduced Transformations in Amorphous Chalcogenides," *J. Optoelectron. Adv. Mat.*, 4 [4] 867–874 (2002).
46. L. Petit, *et al.*, "Effect of IR Femtosecond Laser Irradiation on the Structure of New Sulfo-Selenide Glasses," *Opt. Mater.*, 29 [8] 1075–1083 (2007).
47. B. Frumarova, P. Nemec, M. Frumar, J. Oswald, and M. Vleck, "Synthesis and Optical Properties of the Ge-Sb-S: $PrCl_3$ Glass System," *J. Non-Cryst. Solids*, 256&257 266–270 (1999).